NUREG/CR-0525
ORNL/NUREG/TM-278

Noise Diagnostics for Safety Assessment, Standards, and Regulation Quarterly Progress Report for April–June 1978

D. N. Fry
R. C. Kryter
J. C. Robinson
F. J. Sweeney
W. T. King
E. L. Machado
F. Shahrokhi

Prepared for the U.S. Nuclear Regulatory Commission
Offices of Nuclear Regulatory Research
Nuclear Reactor Regulation, and Standards Development
Under Interagency Agreements DOE 40-551-75 and 40-552-75

OAK RIDGE NATIONAL LABORATORY
OPERATED BY UNION CARBIDE CORPORATION · FOR THE DEPARTMENT OF ENERGY

Printed in the United States of America. Available from
National Technical Information Service
U.S. Department of Commerce
5285 Port Royal Road, Springfield, Virginia 22161

NUREG/CR-0525
ORNL/NUREG/TM-278
Dist. Category R1

Contract No. W-7405-eng-26

INSTRUMENTATION AND CONTROLS DIVISION

NOISE DIAGNOSTICS FOR SAFETY ASSESSMENT, STANDARDS, AND REGULATION QUARTERLY PROGRESS REPORT FOR APRIL-JUNE 1978

D. N. Fry
R. C. Kryter
J. C. Robinson
W. T. King
E. L. Machado
F. Shahrokhi
F. J. Sweeney

Manuscript Completed — November 8, 1978

Date Published — December 1978

NOTICE: This document contains information of preliminary nature. It is subject to revision or correction and therefore does not represent a final report.

Prepared for the
U.S. Nuclear Regulatory Commission
Offices of Nuclear Regulatory Research,
Nuclear Reactor Regulation, and Standards Development
Washington, D.C. 20555
Under Interagency Agreements DOE 40-551-75 and 40-552-75

NRC FIN Nos. B0092, B0723, and B0191

Prepared by the
OAK RIDGE NATIONAL LABORATORY
Oak Ridge, Tennessee 37830
operated by
UNION CARBIDE CORPORATION
for the
DEPARTMENT OF ENERGY

ABSTRACT

Progress, numerical results, and interim conclusions are reported in three study areas funded by the USNRC: the basis for establishment of baseline reactor noise signatures, the assessment of various accelerometer attachment methods employed in loose-part detection systems, and the development of a method for detecting bypass coolant boiling in BWRs.

CONTENTS

1. SCOPE OF PROGRESS REPORT

This report covers the third quarter of FY 1978 and includes selected work in progress under NRC FIN Nos. B0191, B0092, and B0723, which are supported by the Offices of Nuclear Regulatory Research (Division of Reactor Safety Research), Nuclear Reactor Regulation (Division of Operating Reactors), and Standards Development (Division of Engineering Standards), respectively. Since, in many instances, the work is performed under a cost-sharing arrangement among the Divisions, we chose not to single out a "sponsor" for each task.

These quarterly progress reports emphasize numerical results, interim conclusions, and, as desirable, details of the scientific method employed. Most often the general nature, scope, task goals, and reasons for undertaking the work are either presumed or stated in brief terms. Purely descriptive background information is ordinarily omitted.

This quarter's report highlights three work areas: the basis for establishment of baseline reactor noise signatures for BWRs and PWRs, the assessment of various accelerometer attachment methods widely employed in loose-part detection systems, and the development of a method for detecting bypass coolant boiling in BWRs.

2. THE BASIS FOR BASELINE REACTOR NOISE SIGNATURES

D. N. Fry, E. L. Machado, and J. C. Robinson

Purpose. Determine if noise signatures from a few plants can provide the USNRC with generic baseline signatures for use in assessing the condition of nuclear plants.

Method. Compare available BWR and PWR baseline noise signatures from normal plants with signatures from plants having identified problems.

2.1 Introduction

It is evident that the USNRC and its technical consultants could better assess reactor noise abnormalities if baseline noise signatures for every plant were available. However, for a variety of reasons, this is impractical. Therefore, we sought to determine if baseline signatures

obtained at one plant would be applicable to other plants of similar design. If such transferability can be justified technically, we plan to propose to the USNRC that baseline signatures for each *general type* of plant be obtained and the procedures used to obtain the data be documented.

Our study concentrated on *neutron* noise signatures because of the number of PWR and BWR neutron noise baseline signatures available to us. We also have neutron noise signatures from plants with known in-core vibration problems. Using these data, we can show that an abnormal core component vibration can most likely be detected over and above the normal day-to-day and plant-to-plant variations in baseline noise.

We also reviewed a few process variable noise signatures from BWRs and PWRs. At present we have insufficient process variable noise data to make interplant comparisons, but our experience is that process signal analysis is often a useful adjunct to neutron noise analysis in diagnosing core abnormalities.

2.2 BWR Baseline Signatures

Over the past several years, a large number of normal and abnormal neutron noise signatures was obtained during our investigation of in-core instrument tube vibrations in BWR-4 plants. Using these data, we compared normal signatures with a typical abnormal signature from a plant experiencing excessive instrument tube vibrations. Figure 1 shows that the difference in the signature associated with such an in-core abnormality is readily apparent over and above normal plant-to-plant and detector-to-detector signature variations (the shaded area of Fig. 1, as derived from 145 in-core detector signatures from four plants).

We therefore conclude that maintenance of a baseline neutron noise signature file for BWRs need not be a project of impracticably large dimensions and may well prove useful in future assessments of problems in BWRs by the USNRC and its consultants. Since ORNL has an adequate file of BWR-4 signatures, there is no immediate requirement for additional measurements.

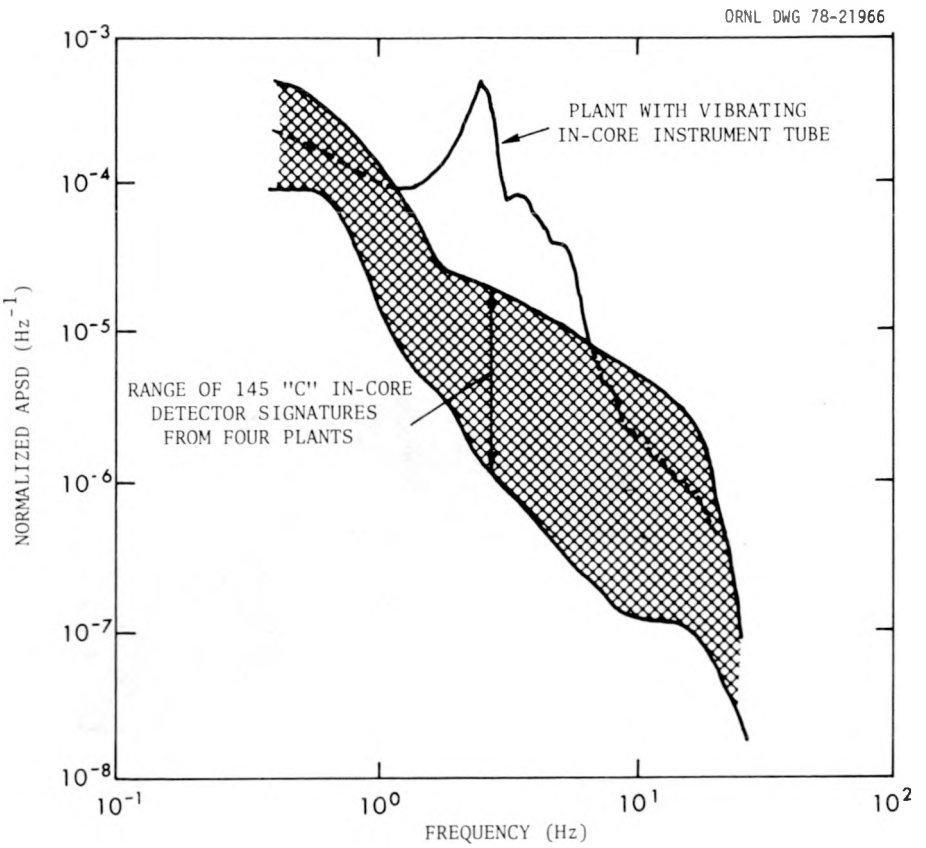

Fig. 1. Comparison of an abnormal signature with a range of baseline signatures for BWR-4s.

2.3 PWR Baseline Signatures

A subcontractor to ORNL has provided neutron noise signatures from 26 ex-core detectors in six PWR plants (2 from each of the 3 U.S. PWR manufacturers). This is a valuable collection of data because it was acquired and reduced in a uniform manner, thus producing a consistent set of signatures that can be intercompared directly. Since the data were obtained from both new and old plants with different amounts of fuel burnup, the signatures represent an essentially random sampling of PWR neutron noise signatures.

As for the BWRs, we compared these signatures with a signature from a PWR having an acknowledged in-core abnormality--a core support barrel with insufficient axial preload force. Figure 2 shows that the signature associated with such an anomaly is significantly different from the corresponding baseline signature (derived from 26 signatures from six plants).

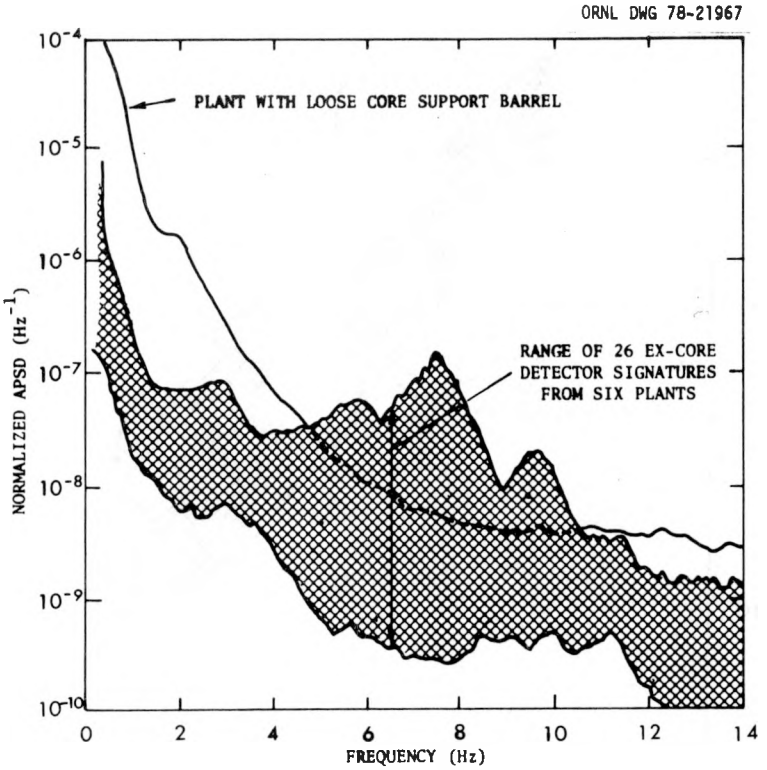

Fig. 2. Comparison of an abnormal signature with a range of baseline signatures for PWRs.

Therefore, as in the case of BWRs, we conclude that the concept of generic baseline neutron noise signatures for PWRs is feasible and potentially useful to the USNRC. Since the PWR data used in this study were not acquired by ORNL and, therefore, are not generally available for our use, we suggest that new data from at least one of each of the three manufacturers' plants be obtained for ORNL's data library.

3. ATTACHMENT CONSIDERATIONS FOR ACCELEROMETERS EMPLOYED IN LOOSE-PART DETECTION SYSTEMS

F. Shahrokhi and R. C. Kryter

Purpose. Identify differences in transduced acoustic signal characteristics resulting from various accelerometer mounting methods.

Method. Compare the time- and frequency-domain responses of the various mountings against that from a reference 10-32 threaded stud mount, using a steel ball freely falling on a steel plate as the impulsive acoustic source.

First Application. Determine best mounting method for accelerometers to be employed in EGCR reactor vessel tests.

Follow-on. Repeat for acoustic emission transducers, as necessary.

3.1 Introduction

Distortions in the signal produced by an accelerometer can be caused by an inappropriate choice of accelerometer mounting method, by incorrect installation technique, or by loss of physical integrity in an otherwise acceptable mount. To determine the nature and magnitude of signal distortions that might thus be expected from various types of mountings and mismountings in loose-part detection system installations, a series of tests was conducted using steel ball impacts on a flat steel machinist's surface plate (44 × 64 × 2 cm). The 10-32 threaded stud mount recommended by the accelerometer manufacturer was designated the "reference" mounting technique, and other mounts and mismounts were then compared to this reference. We found it useful to display the results from these comparisons in both time and frequency domains, as described in the next section.

3.2 Experimental Apparatus and Data Presentation

Table 1 lists the various mounts and mismounts investigated, and Fig. 3 illustrates the geometry of the steel impact plate. The parameters associated with the impact tests are listed in Table 2. The accelerometer, steel ball, impact location, and drop height were unaltered throughout the tests so that the input parameters would be the same, as closely as possible. Plate symmetry was utilized to minimize signal distortions introduced by signal path differences to the mount under test, in comparison to the reference. The experimental setup consisted of a machinist's surface plate, an Endevco model 2236 accelerometer (charge sensitivity ∿66 pC/g), an Endevco model 2730 charge amplifier (frequency response 2 Hz - 50 kHz), and a transient capture oscilloscope with digital storage. A 2-g steel ball was dropped perpendicular to the plate using a magnetic release mechanism. The resultant surface accelerations, with no bandpass restriction other than that imposed by the sensor and amplifier, were digitized at a 2 MHz sampling rate and stored into a single data block of 2048 points per impact.

Table 1. Accelerometer mounts tested

Mount Designation	Description
0	"Reference"; 10-32 threaded stud torqued to 1.92 J
1	Angle hole stud mismount; hole axis ∿10° off perpendicular to surface
2	Short (bottomed) hole stud mismount; hole ∿0.8 mm (1/32 in.) shorter than stud
3	Over-torqued (3.39 J) and under-torqued (1.13 J) threaded stud
4	Cylindrical magnet; holding force ∿111 N.
5	U-shaped channel magnet; holding force ∿333 N.
6	Eight-pole castellated magnet; holding force ∿333 N.
7	Direct pressure mount, with and without silicone grease couplant
8	Commercial 10-32 threaded insulated stud, torqued to 1.92 J

Figure 4 shows the sensed accelerations in nanocoulomb units* vs time after impact for selected tests of Table 2. These highly repeatable transient signals were Fourier transformed to produce the power spectrum (for example, Fig. 5) of each sensed impact. Typical power spectra, discussed in detail in Sect. 3.3, are shown in Figs. 6 through 18. They are particularly enlightening when presented in a normalized form, namely, as a ratio of the acceleration spectrum from the mount under test to that from the reference mount at the same relative position on the plate. Deviations from the "reference" response are thus readily apparent in the figures as departures from the dashed horizontal line at an ordinate value

*The traces of Fig. 4 cannot be converted to "g" (9.80 m/s^2) units through the accelerometer's specified charge sensitivity of 66 pC/g, because that figure is applicable only to the accelerometer's "linear" frequency range, namely, 2 Hz - 8 KHz for the model 2236. The signals of Fig. 4 are wideband.

of unity. The time- and frequency-domain data contain the same information, but the signal distortions introduced by the various mounts are often more clearly perceived in one form or the other. For example, the time-domain plots show the initial wave passage and the time-varying amplitude of the signal particularly well, whereas the normalized frequency spectra show the transfer function (filtration) characteristics of the mount more clearly.

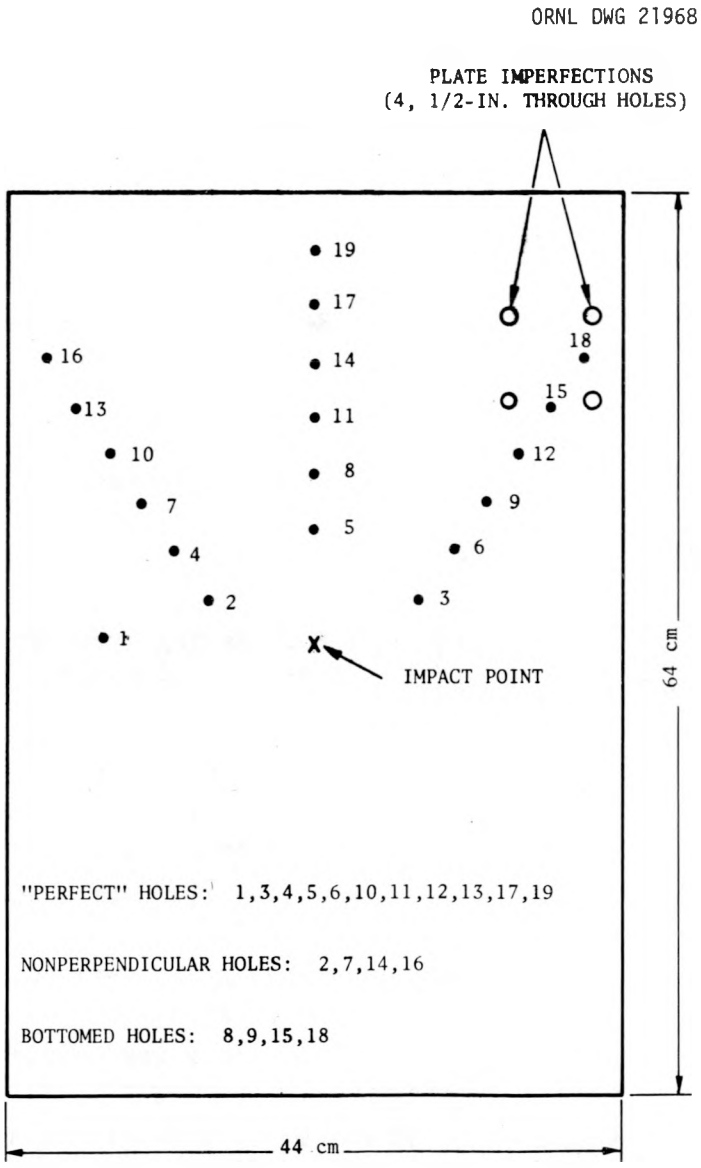

Fig. 3. Accelerometer stud mounting pattern on the impact plate.

Table 2. Accelerometer mounting tests

Impact[a] No.	Accel. Location[b]	Mount Designation[c]	Comments
1	5	0	Reference for impacts 4 and 5
2	14	1	
3	8	2	
4	5	3	Under-torqued stud
5	5	3	Over-torqued stud
6	2	1	
7	3	0	Reference for impact 6
8	13	0	Reference for impact 9
9	15	2	
10	7	1	
11	9	2	
12	between 2 and 4	4	Reference was provided by impact 16
13	between 2 and 4	5	First orientation
14	between 2 and 4	5	Second orientation
15	between 2 and 4	6	
16	4	0	For testing symmetry assumption; also reference for impacts 12-15
17	6	0	
18	4	7	5.9 kg (13 lbf) deadweight and silicone grease couplant
19	4	7	11.8 kg (26 lbf) deadweight and silicone grease couplant
20	4	7	5.9 kg (13 lbf) deadweight; no couplant
21	4	7	11.8 kg (26 lbf) deadweight; no couplant
22	4	8	Reference was provided by impact 16

[a] Steel ball diameter, 0.793 cm; mass, 2.04 g; and drop height, 73.66 cm. Impact energy, 1.47×10^{-2} J (0.011 lbf); momentum, 7.75×10^{-3} N-s; and impact point, geometric center of plate.

[b] See Fig. 3.

[c] See Table 1.

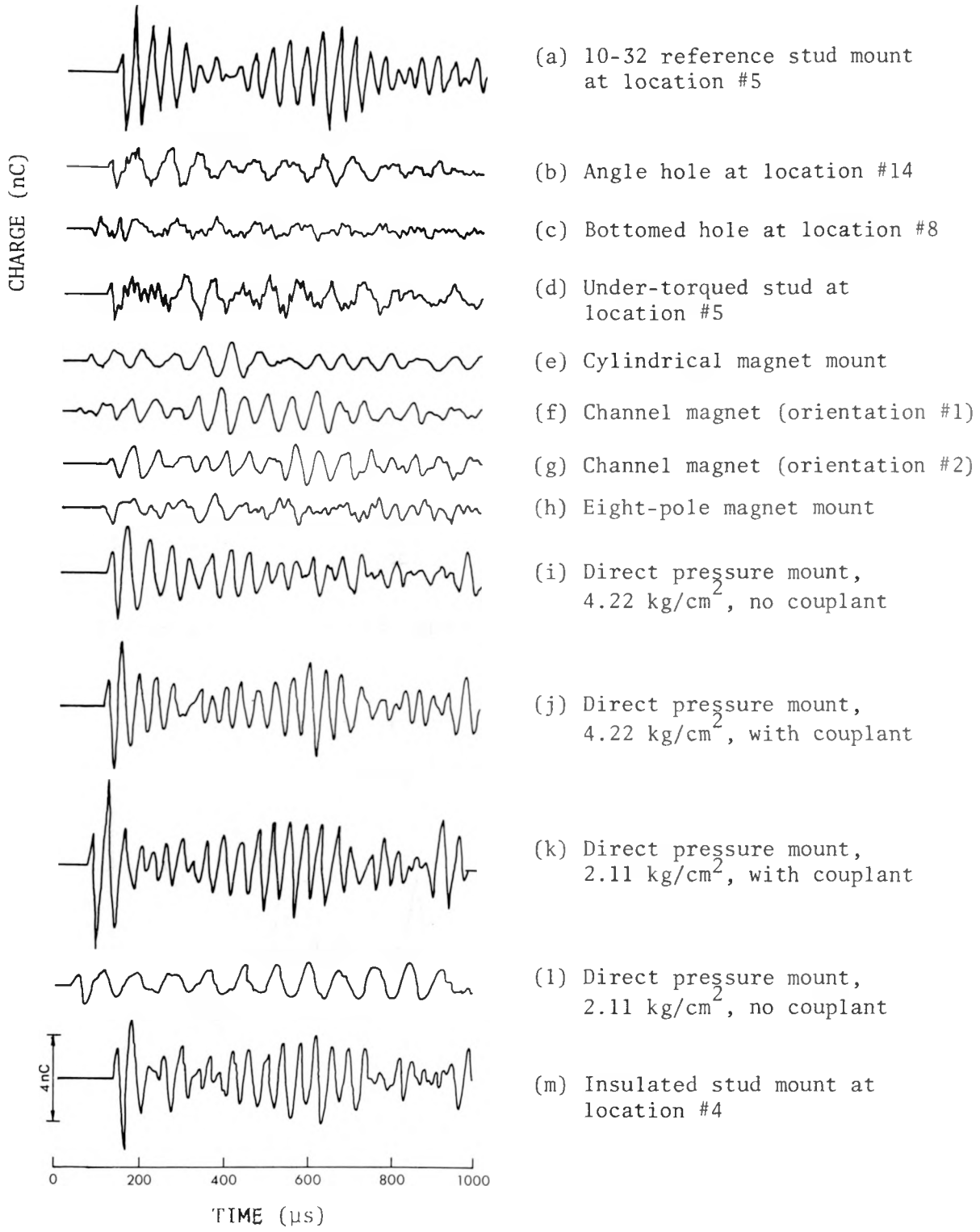

Fig. 4. Time-domain accelerometer responses to the impulse produced by a ball drop, for various accelerometer mounting methods. All traces have the same vertical and horizontal scales.

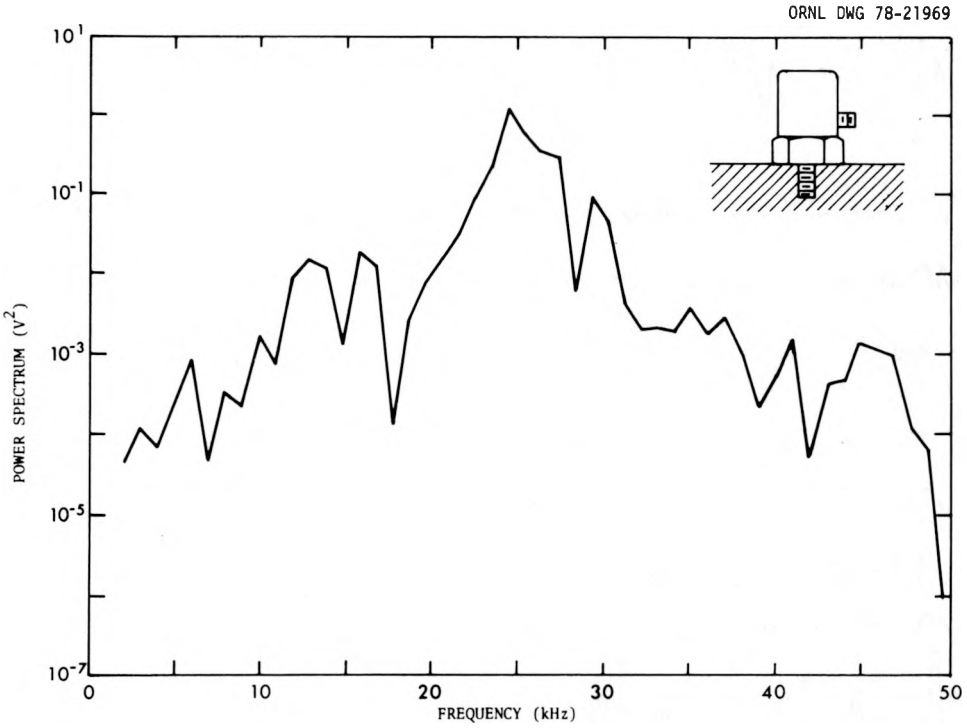

Fig. 5. Acceleration power spectrum for the reference mounting.

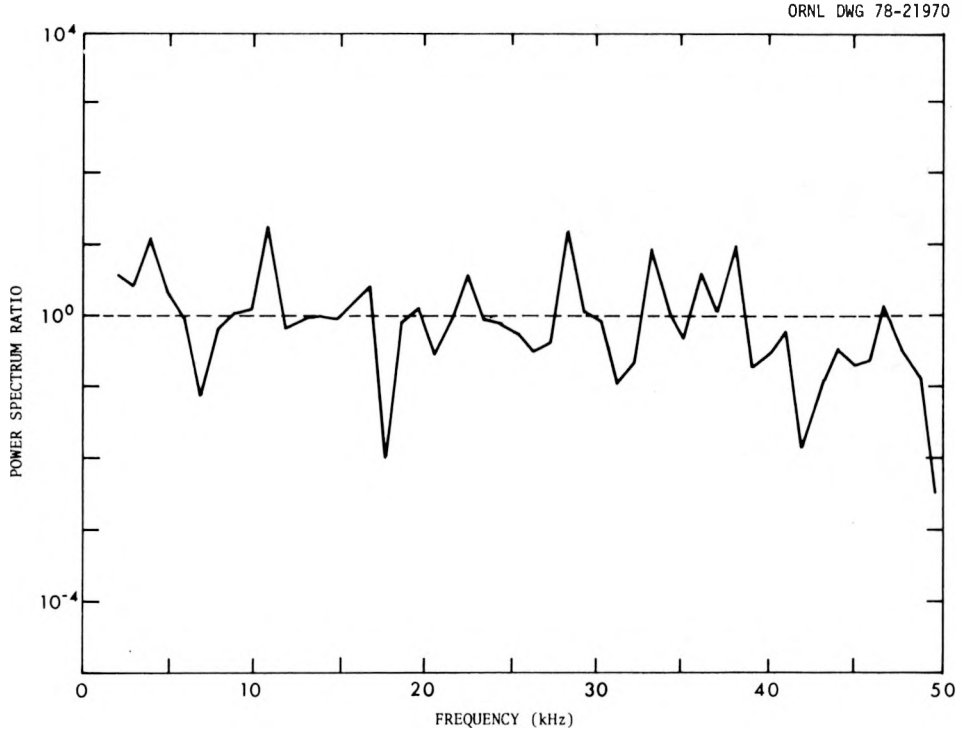

Fig. 6. Ratio of acceleration power spectra at plate positions 4 and 6, illustrating plate response symmetry.

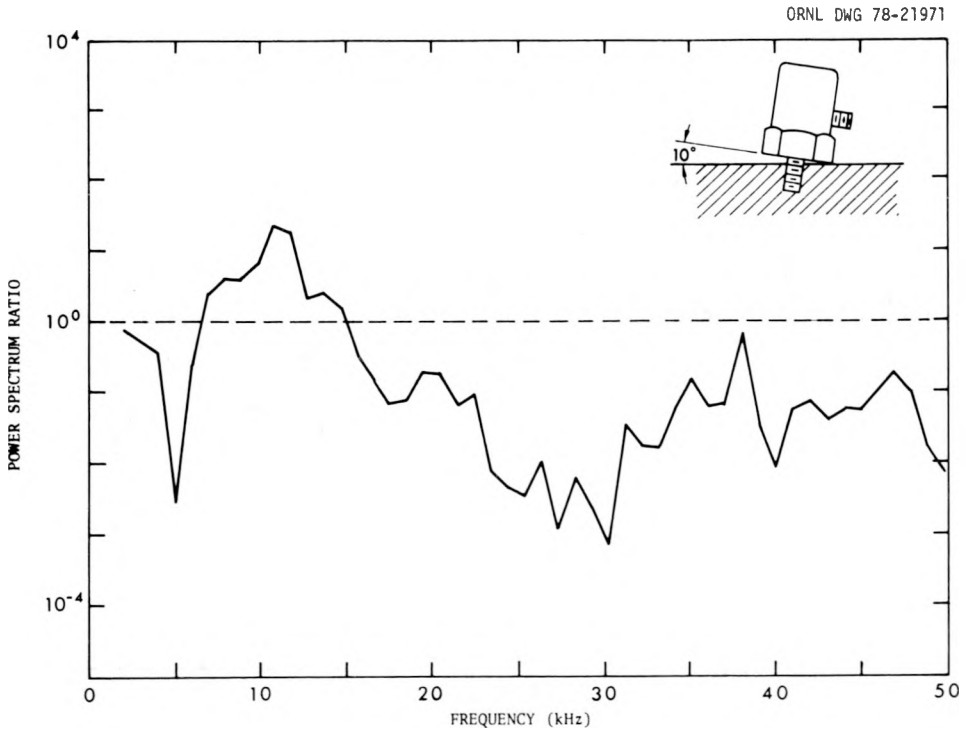

Fig. 7. Response of nonperpendicular hole stud mounting relative to the reference.

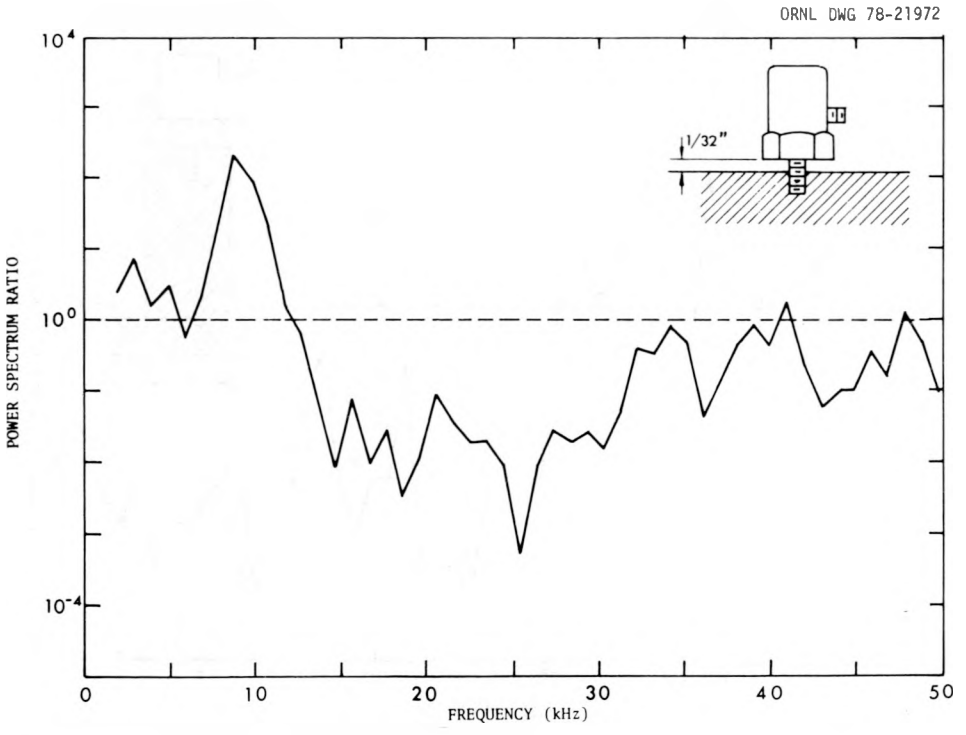

Fig. 8. Response of bottomed hole stud mounting relative to the reference.

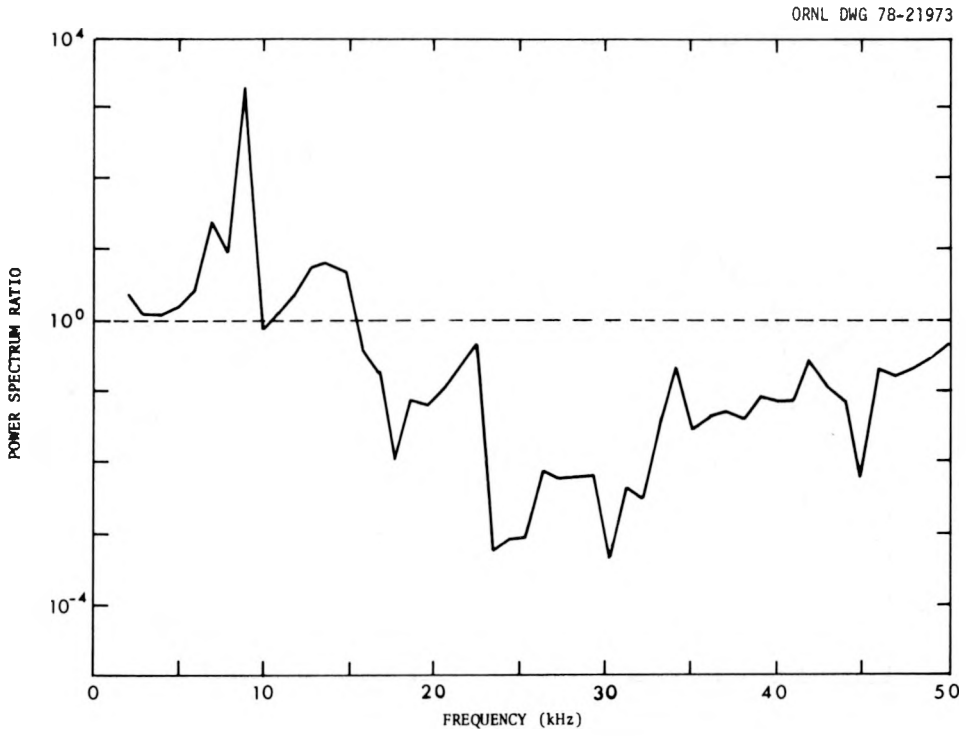

Fig. 9. Response of under-torqued stud mounting relative to the reference.

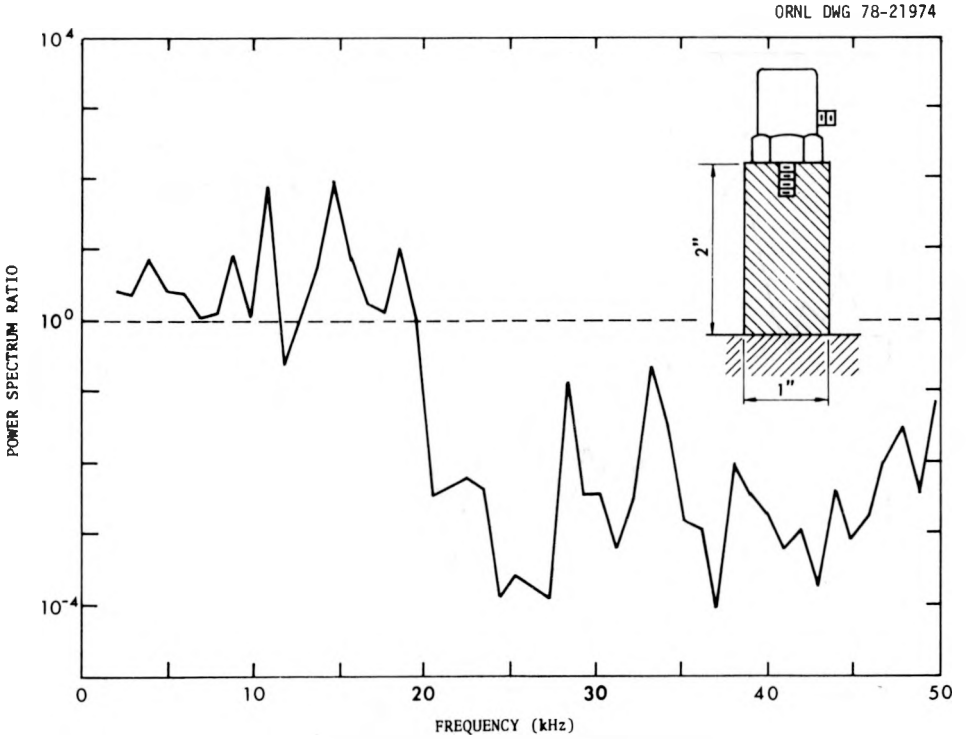

Fig. 10. Response of cylindrical magnet mounting relative to the reference.

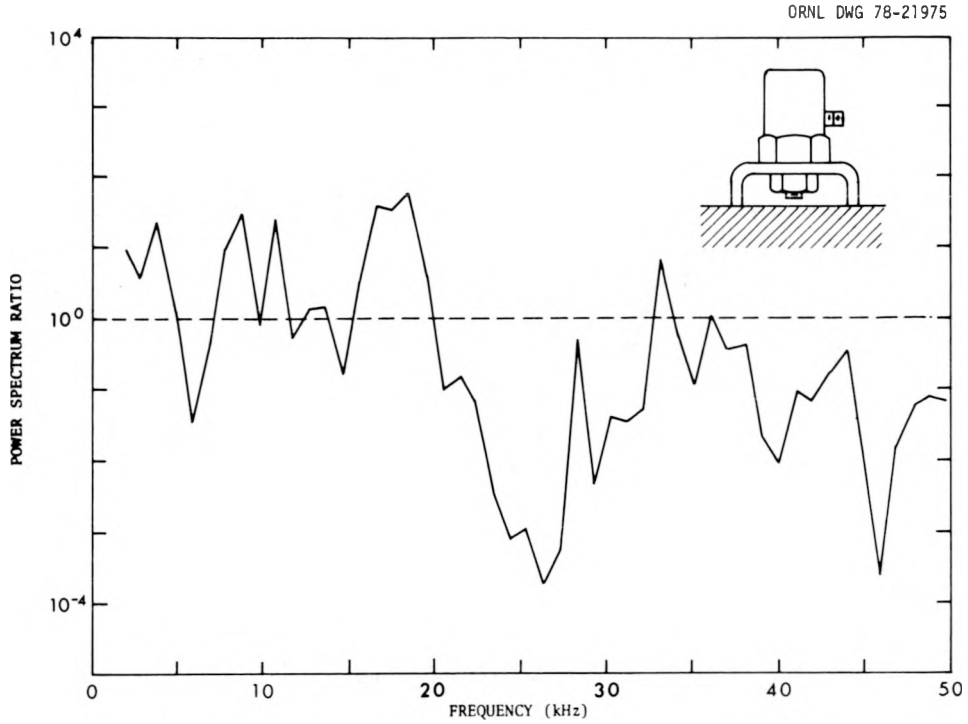

Fig. 11. Response of channel magnet mounting relative to the reference (first orientation).

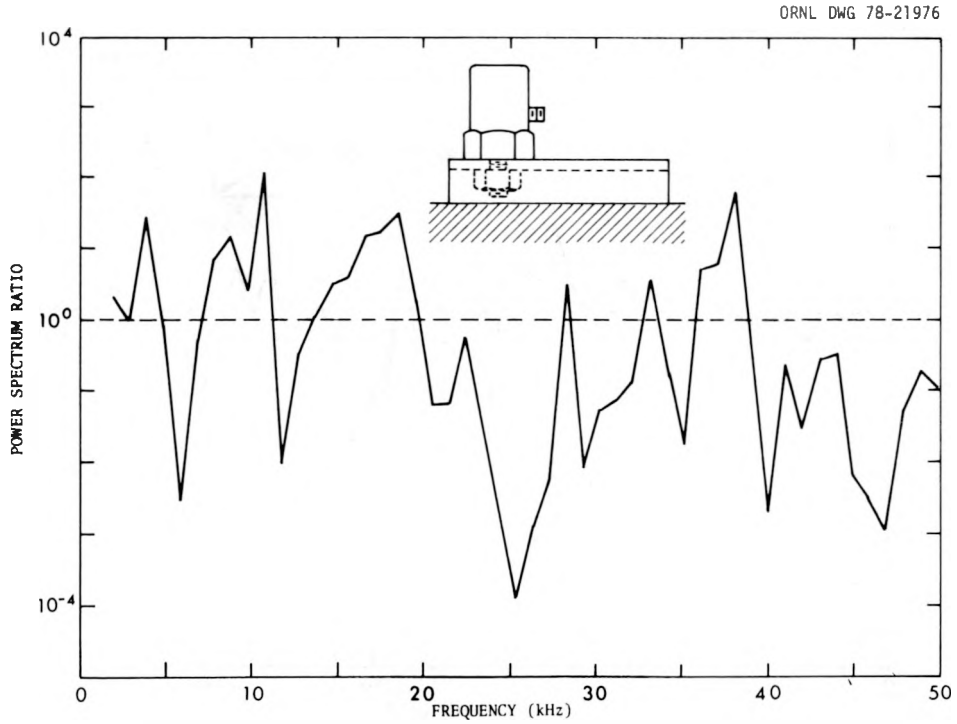

Fig. 12. Response of channel magnet mounting relative to the reference (second orientation).

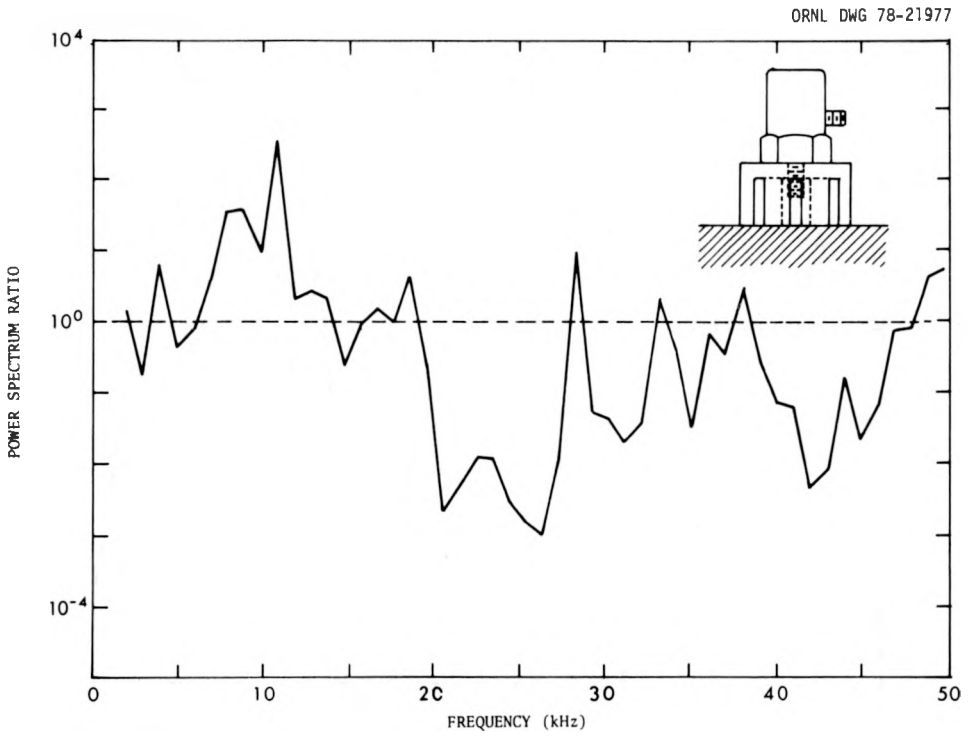

Fig. 13. Response of eight-pole magnet mounting relative to the reference.

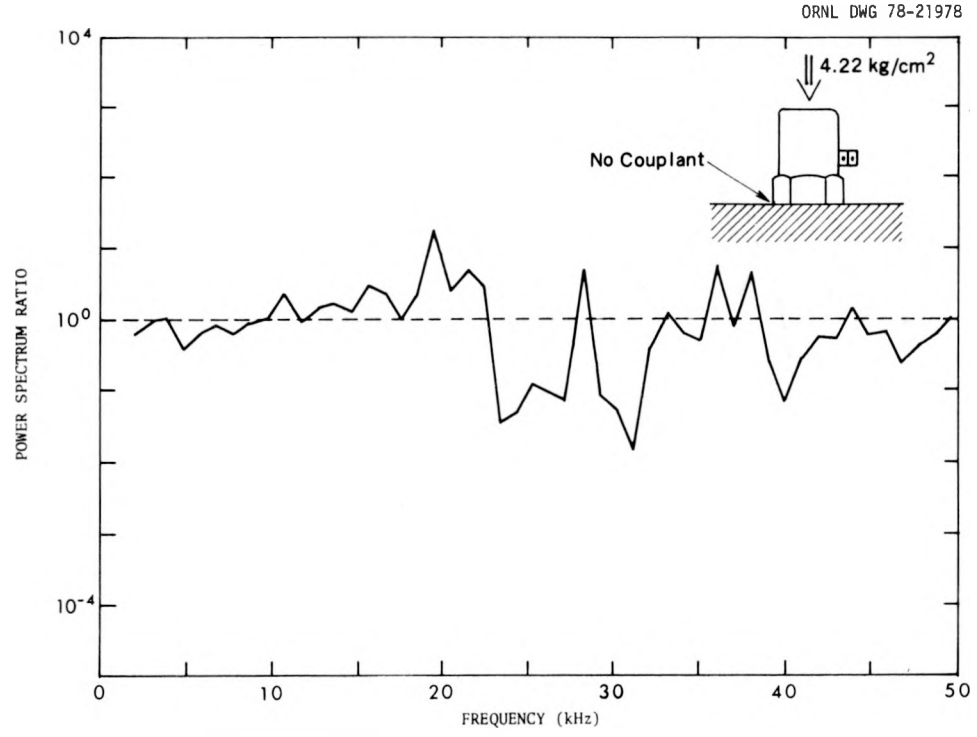

Fig. 14. Response of direct pressure mounting relative to the reference (4.22 kg/cm^2, no couplant).

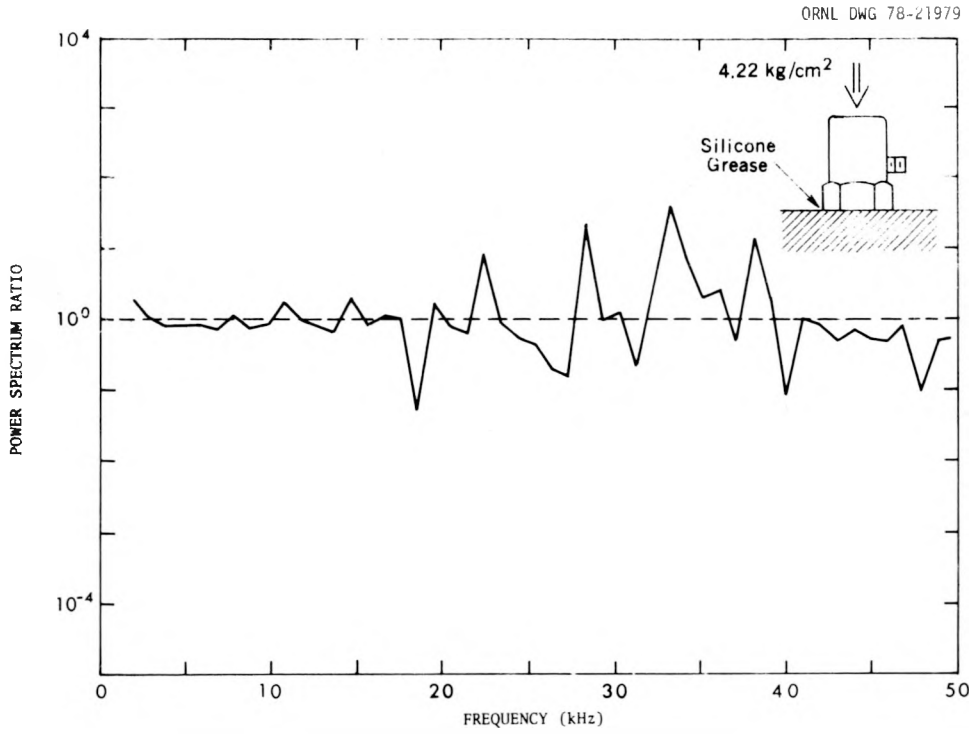

Fig. 15. Response of direct pressure mounting relative to the reference (4.22 kg/cm^2, with couplant).

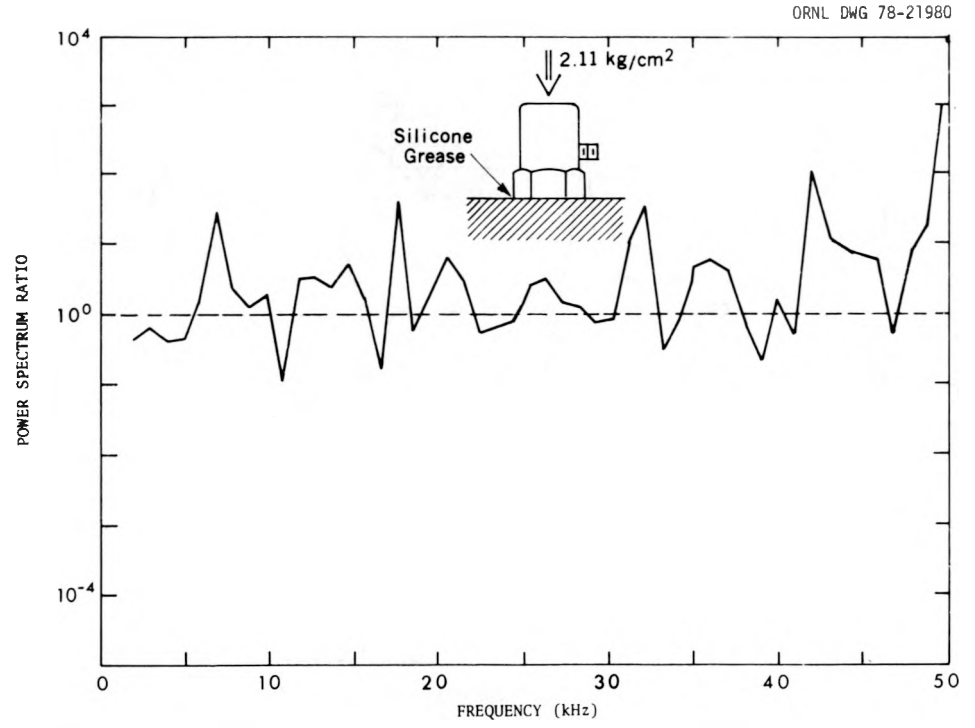

Fig. 16. Response of direct pressure mounting relative to the reference (2.11 kg/cm^2, with couplant).

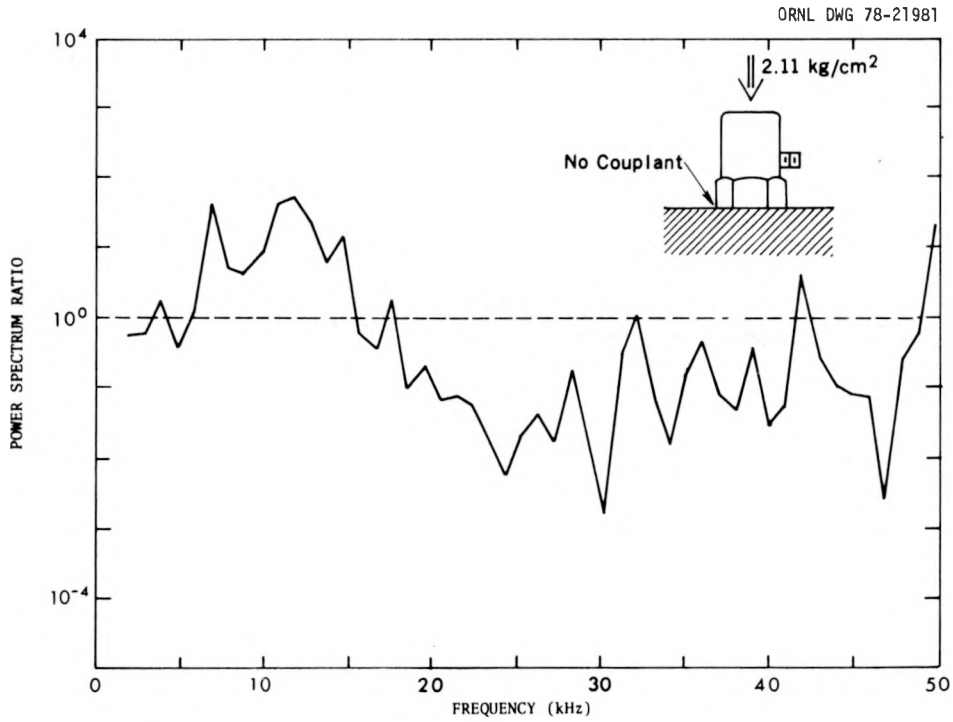

Fig. 17. Response of direct pressure mounting relative to the reference (2.11 kg/cm^2, no couplant).

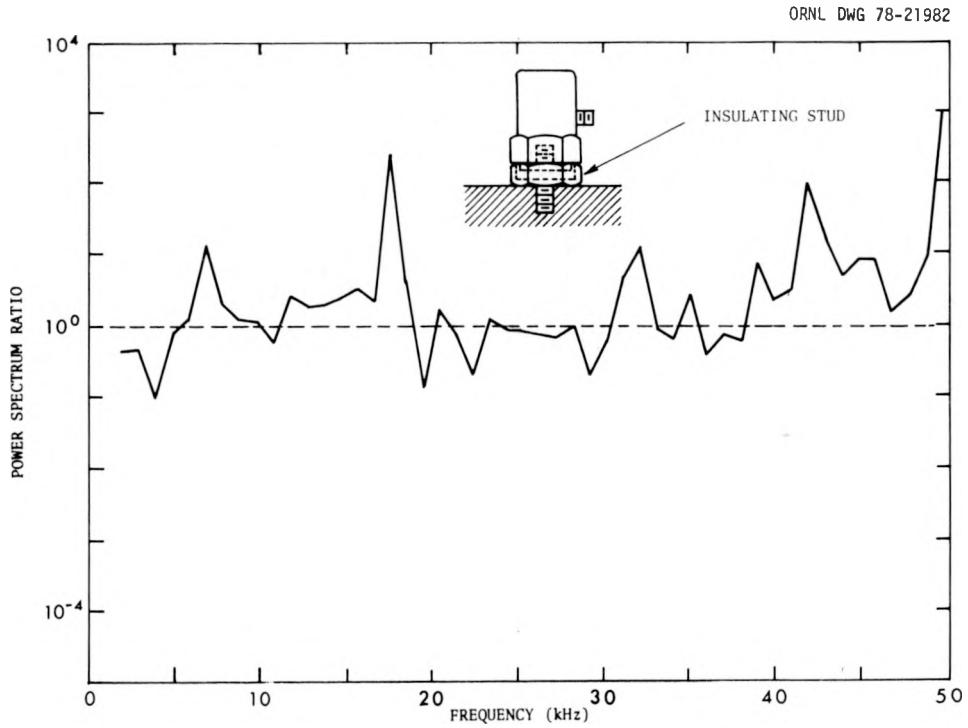

Fig. 18. Response of electrically insulated stud mounting relative to the reference.

3.3 Discussion of Results

To demonstrate that symmetry could be used to simplify the experimental technique, two impacts were performed at two symmetric positions about the major axis of the plate (impacts 16 and 17), and the surface accelerations were compared. Although the surface plate had some inherent asymmetries (Fig. 3), the ratio between the power spectra at these two sensor positions was observed to fluctuate more or less randomly between bounds of about 0.1 and 10 (Fig. 6), with a mean value of roughly unity. We concluded that, to the extent required for subsequent comparisons, response symmetry holds.

The dominant feature of the time domain trace from the reference mount was observed to be smoothly damped oscillations having a period corresponding to the accelerometer's natural (resonant) frequency, roughly 25 kHz (see Figs. 4a and 5).

3.3.1 Angle Hole Stud Mismount

A stud angular mismount was tested by drilling the mounting hole at an angle of $\sim 10°$ off perpendicular. This type of mismount can be anticipated in plant backfit situations where the mounting location of the accelerometer on a reactor structure is not easily accessible. The most prominent effects produced by this mismounting (see Figs. 4b and 7) are an overall loss of signal amplitude (a factor of ~ 2) and a shift of sensed signal power to lower frequencies (7 to 20 kHz) relative to the reference (Fig. 5).

3.3.2 Short (Bottomed) Hole Stud Mismount

This type of mismount, wherein the sensitive face of the accelerometer does not make proper contact with the surface to which it is affixed, can also be expected to occur where accessibility to the mounting location is limited. As in the angle hole case, the time-domain signal amplitude is attenuated a factor of somewhat more than 2 (Fig. 4c) and a frequency-domain distortion also occurs (Fig. 8), in this case a pronounced low-frequency enhancement in the narrow band of ~ 7 to 12 kHz.

3.3.3 Stud Torquing Mismount

The recommended mounting torque for the model 2236 accelerometer is 1.92 J (17 in.-lbf). We performed several tests in which the accelerometer torque was varied from 1.13 to 3.39 J (10 to 30 in.-lbf) and concluded that over-torquing does not appreciably change the time or frequency characteristics of the surface acceleration sensed, whereas under-torquing (<15 in.-lbf for this accelerometer) is accompanied by a significant signal amplitude loss (Fig. 4d), a marked low-frequency enhancement (Fig. 9), and suppression of the accelerometer's resonant behavior in the 23-27 kHz region.

3.3.4 Cylindrical Magnetic Mount

In reactor installations where direct threaded stud mounting to the component of interest is not practical, it has been industry practice to stud mount the accelerometer on a magnet which, in turn, attaches itself to the reactor component (if it is a ferrous material). The data from tests of a cylindrical magnet having a holding force of 111 N (25 lbf) show, relative to the reference mount, a loss of signal amplitude (Fig. 4e) and a general suppression of the higher-frequency surface accelerations (Fig. 10).

3.3.5 U-Shaped Channel Magnetic Mount

We also tested a U-shaped channel magnet, with the accelerometer bolted to the magnet. The magnet had a holding force of ∿333 N (75 lbf). Two orientations of the magnet relative to the direction of the wave propagation were examined. The relative magnitudes of the time signals appeared to be similar (Figs. 4f and 4g), but the initial wave passage signal and the frequency content were different for the two orientations (Figs. 11 and 12). Although perhaps not so corruptive as some of the other mountings tested, the U-shaped channel magnet cannot be viewed as providing a faithful acoustic coupling between the structure and the accelerometer.

3.3.6 Eight-Pole Magnet

An accelerometer bolted to an eight-pole magnet (333 N holding force) produced time-domain amplitude characteristics similar to those for the other magnets (Fig. 4h), but the initial wave formation and frequency characteristics were distinct (Fig. 13). Compared to the reference mount, there was a trough in the 20-25 kHz region and a crest in the 7-12 kHz region.

3.3.7 Direct Pressure Mount

Direct pressure mounting of the accelerometer (often accomplished at reactors with taut steel bands or clamps) was also examined (Figs. 4i-4ℓ; 14-17). Since the accelerometer case is not designed to transmit the large forces that would be required to achieve good acoustic coupling between two dry surfaces, the use of a liquid or gel couplant between the accelerometer face and the mounting surface is almost a necessity in this type mounting. Its presence results in signal amplitude and frequency transfer characteristics that closely approach the reference threaded stud mount (Figs. 4j and 4k, 15, and 16). Two pressures, $\sim$2.11 and $\sim$4.22 kg/cm^2 (30 and 60 lbf/in.^{2}), were applied by placing a dead-weight atop the accelerometer, but the resulting variations in the transfer characteristics were judged to be insignificant, so long as the couplant was present. Without the couplant, however, signal distortion was appreciable, particularly for the lower pressure case (Figs. 4ℓ and 17).

3.3.8 Insulated Stud Mount

Electrically insulated, threaded studs are often used in loose-part detection systems to avoid ground loops. Our tests showed that the distortions introduced by a commercial insulated stud were not pronounced (Fig. 4m), except for a slight emphasis of frequencies >40 kHz (Fig. 18).

3.4 Concluding Remarks

Any obstruction (in the form of an indirect mount) interposed between the structural surface waves and the sensing surface of the accelerometer acts as a mechanical filter and thus, to some extent, it can be expected to modify the electrical signal produced by the transducer. Depending upon the application, this modification may or may not be important. If the frequency-dependent transfer function of the mount is constant with time and independent of the magnitude of the acoustic wave being sensed, the distortions introduced by the mount can be removed, if desired, by well-known signal processing methods. Alternatively, measurement of the mount's signal transfer function can serve to quality assure the accelerometer installation.

For all mismountings tested, perhaps the most notable effects were (1) a significant loss ($\sim$2) in peak waveform amplitude, and (2) a selective loss of the higher signal frequencies, often accompanied by an accentuation of certain lower frequency bands. From the standpoint of loose-part detection, the first effect is probably the more important since, for a simple threshold discriminator logic system, mismounting would result in a direct loss of loose-part detection sensitivity, whereas the second effect would most likely degrade only the system's selectivity for metallic impacts. These generalizations apply specifically to *wideband* loose-part detection systems; narrowband systems could conceivably be affected to a lesser degree, depending on the frequency bands selected, and would require analysis on an individual case basis.

Since acoustic couplants can obviously greatly reduce the distortions and signal losses accompanying accelerometer mismounting, the practicality of their use in the high-temperature and high-radiation environments encountered in loose-part detection applications might be worthy of further study.

4. A METHOD FOR DETECTING BYPASS COOLANT BOILING IN BOILING WATER REACTORS*

D. N. Fry
E. L. Machado
W. T. King
F. J. Sweeney

4.1 Summary

Fluctuating signals from in-core neutron detectors in four boiling-water reactors (BWRs) were analyzed to better understand the differences in the amplitude of neutron noise coherence spectra previously reported.[1] This investigation has led to a possible method for detecting boiling of bypass water in BWRs. A significant decrease in the coherence between signals from C and D local power range monitor (LPRM) detectors was observed when the core bypass coolant flow was reduced by plugging the holes in the core support plate--a modification made to reduce in-core instrument tube vibrations.

We hypothesized that reduced bypass flow caused boiling in the bypass region and that the onset of bypass boiling was at an elevation between the two detectors mentioned. Additional fluctuations in the downstream detector signals caused by bypass voids are not correlated to the upstream detector signals, thereby decreasing the coherence between the two signals.

All four plants included in the analysis had plugged bypass coolant holes. Three plants had only leakage flow in the bypass region, which is 6-8% of the total core flow. The fourth plant had coolant holes drilled in the lower tie plates of the fuel bundle, which increased the bypass flow to 10-12%. We analyzed simultaneous tape recordings of signals from the four in-core neutron detectors at each of the 31 or 43 LPRM locations in each plant. The detectors designated A, B, C, and D are located 18, 54, 90, and 126 in., respectively, from the fuel bundle inlet.

Figure 19 compares typical, normalized auto-power spectral densities (APSDs) of the C and D detector signals and their coherence in plants with

---

*Summary accepted by the American Nuclear Society for presentation at the Winter Meeting in Washington, D.C., November 12-17, 1978.

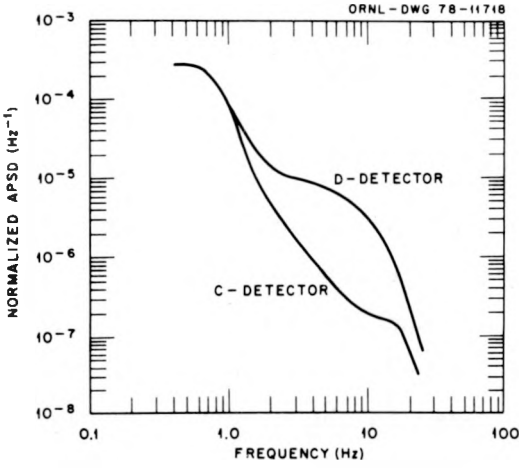

(a) Power spectrum for bypass flow of 6-8%

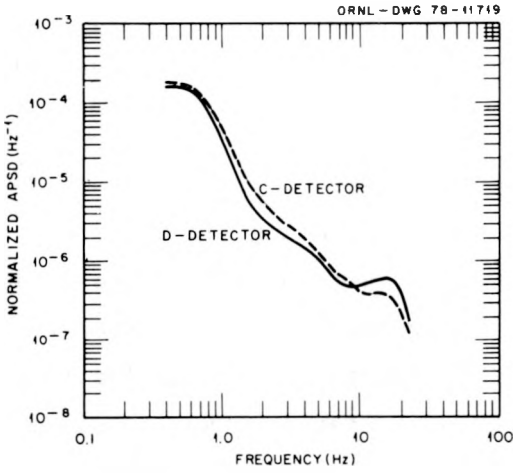

(b) Power spectrum for bypass flow of 10-12%

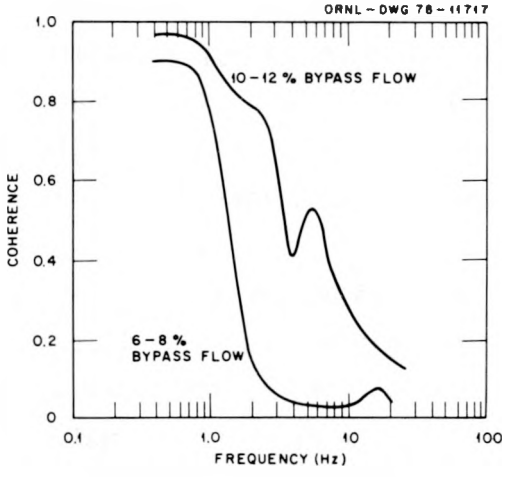

(c) C-D detector coherence spectra for different bypass flows

Fig. 19. BWR-4 in-core neutron noise as a function of bypass flow.

6-8% bypass flow with APSDs and coherence typical of the plant with 10-12% bypass flow. With 6-8% bypass flow, the amplitude of the noise spectrum of the D detector from 1 to 10 Hz is almost an order of magnitude larger than that of the C detector (Fig. 19a), whereas with 10-12% bypass flow, the C and D detector noise spectra are similar in the same frequency range (Fig. 19b).

Normally, the major contributors to neutron noise in the frequency range from 1 to 10 Hz are steam voids in the fuel channel boxes. Most of these voids are formed below the C and D detectors, such that both detectors detect some of the same voids. Therefore, the C and D detector signals are highly coherent, as in the case of the plant with 10-12% bypass flow (Fig. 19c). In fact, other investigators[2,3] have used these correlated neutron noise signals to infer the steam-void velocity and void fraction in the channel boxes in operating BWRs.

On the other hand, the added noise at the D detector location (presumably due to void formation in the bypass flow between the C and D detectors) in plants with 6-8% bypass flow is not correlated with the C detector signal, thus resulting in the low coherence between the C and D detector signals (Fig. 19c).

A complicating factor in our analysis was that the plant with the greater bypass flow also had a different fuel design (8 × 8 fuel pin array, instead of 7 × 7). However, because the A, B, and C detector signatures are similar in plants with either type of fuel, we do not believe that this different fuel design caused the difference in the noise at the D detector location.

To test our hypothesis of bypass boiling, we performed a thermal-hydraulic calculation to estimate the elevation at which bypass boiling occurs as a function of the bypass flow rate. The fuel bundle coolant temperature was calculated using a code developed by Mills,[4] with a typical normalized traversing in-core probe (TIP) trace providing the power shape. The fuel bundle temperature and flow rates, together with the bypass flow rates and inlet conditions, were used to calculate the amount of heat conducted from the fuel bundle coolant, through the fuel box wall, to the bypass coolant. The heat contribution from fast-neutron moderation in the bypass coolant was included, based on the work by

Carlson.[5] From these heat sources, we estimated the temperature of the bypass coolant as a function of elevation and bypass flow. Figure 20 shows that for 6-8% bypass flow the average bypass coolant temperature reached saturation temperature (bulk boiling) at ∿100-126 in. (between the C and D detectors), whereas for bypass flows greater than ∿9%, the saturation temperature was not reached below the core outlet.

We conclude that reduced bypass flow caused boiling in the bypass region, and this boiling caused the observed differences in neutron noise signatures. These results suggest that, with the aid of the TIPs, the axial location at which bypass boiling occurs can be determined. With additional measurements and more refined thermal-hydraulic calculations, it might be possible to infer the bypass void fraction, which is of interest in the safety evaluation of BWRs.

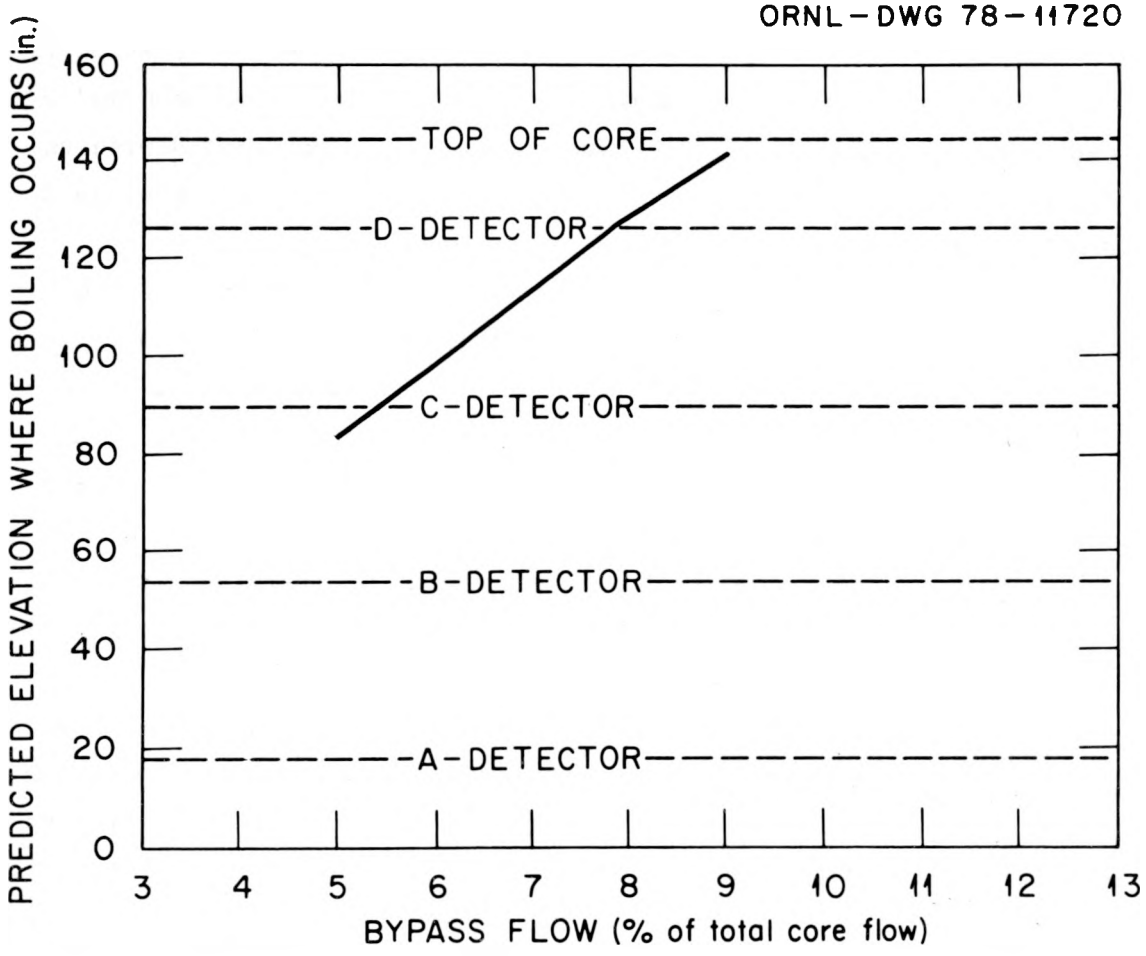

Fig. 20. Core elevation where bypass coolant bulk boiling is predicted to occur.

4.2 References

1. M. V. Mathis, C. M. Smith, and D. N. Fry, "Characterization Studies of BWR-4 Neutron Noise Analysis Spectra," *Trans. Amer. Nucl. Soc.* 27, 677-678 (1977).

2. M. Ashraff Atta et al., "Determination of Void Fraction Profile in a Boiling Water Reactor Channel Using Neutron Noise Analysis," *Nucl. Sci. Eng.* 66(2), 264-268 (1978).

3. G. Kosály et al., "Investigation of the Local Component of the Neutron Noise in a BWR and Its Application to the Study of Two-Phase Flow," *Proc. OECD(NEA) CSNI/NEACRP Specialists' Mtg. Reactor Noise (SMORN II)*, CSNI Report No. 22/NEACRP-U-81, Pergamon Press, Ltd., Oxford, England (1977).

4. L. Mills, "An Investigation of the Thermal Aspects of a Boiling Water Reactor," M. S. Thesis, University of Tennessee, Knoxville (March 1968).

5. R. G. Carlson and D. R. Gott, "Bypass Flow Distribution in a Boiling Water Reactor," *Nucl. Technol.* 33, 161-173 (1977).

NUREG/CR-0525
ORNL/NUREG/TM-278
Dist. Category R1

Internal Distribution

1-5. R. S. Booth
6. W. B. Cottrell
7. M. H. Fontana
8. D. N. Fry
9. W. O. Harms
10. H. N. Hill
11. W. T. King
12. R. C. Kryter
13. E. L. Machado
14. F. R. Mynatt
15. F. H. Neill
16. L. C. Oakes
17. K. R. Piety
18. C. W. Ricker
19. G. S. Sadowski
20. F. Shahrokhi
21-22. Myrtleen Sheldon
23. C. M. Smith
24. F. J. Sweeney
25. D. B. Trauger
26. G. D. Whitman
27. Patent Office
28-29. Central Research Library
30. Y-12 Document Reference Section
31-33. Laboratory Records Department
34. Laboratory Records (RC)

External Distribution

35-42. Director, Office of Nuclear Regulatory Research, U. S. Nuclear Regulatory Commission, Washington, DC 20555

43. Assistant Manager for Energy Research and Development, DOE, ORO

44. W. S. Farmer, Reactor Safety Research Division, USNRC, Washington, DC 20555

45. G. C. Millman, Office of Standards Development, USNRC, Washington, DC 20555

46. H. J. Vander Molen, Office of Nuclear Reactor Regulation, USNRC, Washington, DC 20555

47. Public Document Room, 1717 H-Street, USNRC, Washington, DC 20555

48-267. Given distribution as shown in category R1 (25 copies - NTIS)

268. J. C. Robinson, Technology for Energy Corp., Knoxville, TN 37922